On the influence of the preparation routes of NiMgAl-mixed oxides derived from hydrotalcite on their CO2 methanation catalytic activities

Minh Nguyen-Quang, Federico Azzolina-Jury, Bogdan Samojeden, Monika Motak, Patrick da Costa

Available online at www.sciencedirect.com

ScienceDirect

journal homepage: www.elsevier.com/locate/he

On the influence of the preparation routes of NiMgAl-mixed oxides derived from hydrotalcite on their CO_2 methanation catalytic activities

Minh Nguyen-Quang [a,b,c], *Federico Azzolina-Jury* [a,*], *Bogdan Samojeden* [b], *Monika Motak* [b], *Patrick Da Costa* [c]

[a] *Laboratoire Catalyse et Spectrochimie (LCS), CNRS-ENSICAEN-Université de Caen, 6 boulevard du Maréchal-Juin, 14000 Caen, France*

[b] *Faculty of Energy and Fuels, AGH University of Science and Technology, Kraków, Poland*

[c] *Institut Jean le Rond d'Alembert, Sorbonne Université, CNRS UMR 7190, Saint Cyr l'Ecole, France*

HIGHLIGHTS

- The hydrolysis of urea was applied to successfully synthesize NiMgAl mixed oxides catalyst (NMA-UH).
- NMA-UH facilitates CO_2 conversion at lower temperatures compared to catalysts synthesized via traditional routes.
- Adding urea to the synthesis liquid generates more layers in the catalyst framework and increases its surface area.
- Its hydrolysis in the medium results in a significant improvement in total basicity and weak-medium site distribution.

GRAPHICAL ABSTRACT

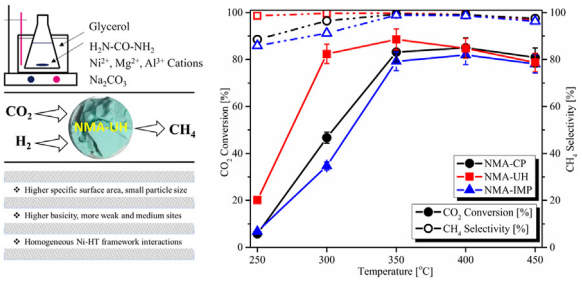

ARTICLE INFO

Article history:
Received 13 June 2022
Received in revised form
22 August 2022
Accepted 28 August 2022
Available online xxx

ABSTRACT

In this work, a series of NiMgAl oxides (NMA) derived from hydrotalcite catalysts were prepared via co-precipitation (NMA-CP), urea hydrolysis (NMA-UH), and impregnation (NMA-IMP) techniques, then subsequently tested for CO_2 methanation. The well-defined synthesis of derived hydrotalcite mixed oxides was confirmed by physicochemical characterizations including XRD, SEM, BET, H_2-TPR and CO_2-TPD. The preparation methods showed a substantial influence on the structure and thermal activity of catalysts. Indeed, the NMA-UH catalyst demonstrated a high and stable catalytic activity in terms of CO_2

* *Corresponding author.*
E-mail address: federico.azzolina-jury@ensicaen.fr (F. Azzolina-Jury).

https://doi.org/10.1016/j.ijhydene.2022.08.278

Please cite this article as: Nguyen-Quang M et al., On the influence of the preparation routes of NiMgAl-mixed oxides derived from hydrotalcite on their CO_2 methanation catalytic activities, International Journal of Hydrogen Energy, https://doi.org/10.1016/j.ijhydene.2022.08.278

Keywords:
NiMgAl-Hydrotalcite mixed oxides
Co-precipitation
Urea hydrolysis
Ni impregnated MgAl-Hydrotalcite
CO_2 methanation

conversion and CH_4 selectivity, with ca. 82.3% and 99.8% (GHSV = 12,000 h^{-1}, H_2/CO_2 = 4/1) respectively, at 300 °C. This is mainly due to its large specific surface area, small Ni-particle size, and higher basicity.

Introduction

According to the newly issued International Energy Outlook, global energy consumption is anticipated to rise by 48% between 2012 and 2040 [1]. Increasing energy consumption currently jeopardizes world energy security and puts the environment under strain. The main issues in terms of climate change to concentrate on are reducing greenhouse gas emissions and increasing the efficient usage of renewables at the same time [2]. Using CO_2 as a cheap and plentiful chemical feedstock has received much interest; it has many benefits in generating value-added chemicals and liquid fuels (e.g., methane, methanol). This is a promising strategy due to its potential to utilize exhausted CO_2.

The CO_2 methanation process developed by Sabatier and Senderens (Eq. (1)), first introduced in 1902, is regarded among the most advanced technologies for recovering CO_2 and meeting the growing need for energy resources [3] and thus can be a long-term answer to escalating energy demands.

$$CO_2 + 4H_2 \rightarrow CH_4 + 2H_2O,\ \Delta H^0_{298K} = -165 kJ/mol \quad \text{(Eq. 1)}$$

First and foremost, the power-to-gas strategy offers the possibility of large-scale CO_2 recycling in tandem with the use of a large amount of renewable energy to produce methane. Second, space agencies such as NASA have also highlighted methanation as a crucial reaction for long-term space exploration missions. This reaction is presented as the key parameter that will eventually define its technological and economic feasibility on Earth and in Space [4]. However, pressure and temperature dramatically impact the reaction equilibrium because the Sabatier reaction (Eq. (1)) is considerably exothermic and volume-reducing. In order to reach high CO_2 conversion, thermodynamically, it is preferential to run the reaction at low temperatures. Nevertheless, low temperature implies slow reaction kinetics; therefore, looking for efficient catalysts that support for the reaction to operate productively under moderate conditions is unavoidable.

The Ni-based catalyst is presently recognized as a promising catalyst-base for CO_2 methanation because of its satisfactory catalytic activity at high temperatures and low cost [5–7]. When the reaction temperature turns lowered, however, its catalytic activity drops. Recently, the development of Ni-based catalysts found hydrotalcite (HT) as a promising material for CO_2 conversion [8,9]. The formula of HT-like compound is presented below (Eq. (2)):

$$OH)(OH)(OH)_2]^{x+}[(A^{n-}_{x/n})^{x-}.mH_2O] \quad \text{(Eq. 2)}$$

Where $M^{(II)}$- the divalent cations such as Mg^{2+}, Ni^{2+}; $M^{(III)}$- the trivalent cations like Al^{3+}; A^{n-}- compensating anions (CO_3^{2-}, SO_4^{2-}, NO_3^-), is an interlayer n valent anion; and x varies between approximately 0.25 and 0.33; m-is the content of co-intercalated water. Hydrotalcite, upon calcination, turns into oxide-form through several changes: dehydration, dehydroxylation, and the loss of compensating anions, which generate basic characteristics and a weakly crystalline structure [10,11]. These oxides own a smaller particle size, a larger specific surface area, uniform metal inter-dispersion, and greater sintering resistance than corresponding supported catalysts. The chemical compositions, preparation methods, and treatment parameters influence the surface basic, particle size, and/or redox features [12–14]. These are all crucial parameters to define a suitable catalyst. Many approaches, such as co-precipitation [15–17], sol-gel [18–20] and hydrothermal synthesis [21–23], reconstruction [24,25], microwave irradiation [26–29], biomineralization [30], have been reported for the synthesis of HT. Choosing the synthesis routes is a pivotal step depending on the requirements of the purpose of usage.

The synthesis of HT materials via urea hydrolysis has been recognized as a new technique. So far, however, only few works have been dedicated to synthesizing hydrotalcite via such a technique. Available works could be listed as MMgAl-HT where M = Fe, Co, Ni, Cu, or Zn [31], or M(II)M′ (II)Al-HT with M(II) and M' (II) = Fe, Co, Ni, or Zn [32], or Ru–NiMgAl-HT [33]. The others addressed either the synthesis of MgAl-HT [22,34,35] or NiAl-HT [36,37], with most of the interest focusing on the catalysts' synthesis parameters and characterizations; the applications for catalytic-chemical processes, nevertheless, are still limited. More importantly, NiMgAl-HT synthesized via urea hydrolysis method has never been reported for a catalytic test of CO_2 methanation before.

This work, therefore, is dedicated to the synthesis of NiMgAl-HT via urea hydrolysis route and its application for CO_2 methanation compared to traditional co-precipitation and impregnation catalysts. First, NiMgAl-HT material (NMA) was synthesized by co-precipitating Ni, Mg, and Al-precursors. Following the same synthesis procedure, MgAl-HT was also prepared. MgAl-HT as a support was used for impregnating purpose of Ni as active sites. On the other hand, NMA was synthesized via the urea hydrolysis route for comparative study. These three catalysts were then tested under the 250–450 °C range of CO_2 methanation conditions.

Experimental

Catalyst synthesis and characterizations

Three strategies of synthesis were chosen in this study:

Please cite this article as: Nguyen-Quang M et al., On the influence of the preparation routes of NiMgAl-mixed oxides derived from hydrotalcite on their CO_2 methanation catalytic activities, International Journal of Hydrogen Energy, https://doi.org/10.1016/j.ijhydene.2022.08.278

(i) *Co-precipitation*: The NiMgAl-HT was synthesized through co-precipitation at constant pH from an aqueous solution containing Ni acetate, Mg and Al nitrate precursors $[M^{(III)}/(M^{(II)} + M^{(III)}] = 0.25$, 15 wt% Ni loading) following [15,38]. Shortly, solution A contains 1 M of Ni^{2+}, Mg^{2+} and Al^{3+} cations using acetate salts of nickel $(Ni(Ac)_2.6H_2O)$ and nitrate salts of magnesium and aluminum $(Mg(N)_2{\cdot}6H_2O$, $Al(N)_3{\cdot}9H_2O)$ at a molar ratio $[Al^{3+}/(Ni^{2+} + Mg^{2+} + Al^{3+})]$ of 0.25. Solution B was prepared by dissolving a proper quantity of Na_2CO_3 in water to achieve the concentration of CO_3^{2-} of 1.0 M. Solution A was added dropwise into solution B under vigorous stirring at the constant temperature of 65 °C. The mixture was aged for 1 h, keeping the pH 9.5–10 throughout the synthesis process by NaOH 1 M. After vacuum filtering and washing with deionized water to pH = 7, the obtained slurry was dried overnight at 80 °C and calcined at 550 °C for 5 h with a 5 °C/min heating ramp. The complete catalyst was named NMA-CP.

(ii) *Impregnation*: Using the same procedure, MgAl-HT was synthesized separately as a support with $[Al^{3+}/(Mg^{2+} + Al^{3+})] = 0.25$. Nickel, as active sites, was introduced onto the MgAl-HT by impregnation with 15 wt% loading (NMA-IMP).

(iii) *Urea Hydrolysis*: The synthesis of NiMgAl-HT via urea hydrolysis followed the procedure reported by M. Adachi-Pagano et al. [34]. Some synthesis parameters such as temperature, aging time, and the medium were varied by researchers [31,36] in which the hydrolysis was thought to be faster at 100–110 °C, and the requirement of aging time was 10–48 h in an autoclave, or 4 days aging at 130 °C [37]. In this study, however, the same temperature as the co-precipitation procedure during the synthetic step was applied for comparative study as described herein. First, a glycerol-oil bath was set up and heated up to 65–70 °C. 100 ml of deionized water, 20 ml of a metal salts solution ($Ni^{2+} + Mg^{2+} + Al^{3+} = 1$ M, $[Al^{3+}/(Ni^{2+} + Mg^{2+} + Al^{3+})] = 0.25$) and urea, $[urea/(Ni^{2+} + Mg^{2+} + Al^{3+})] = 3.3$, were added into a 1 dm^3-triangle flask and stirred at room temperature. It could be seen that the solution was transparent and clear when stirred at 25 °C. Afterward, the flask was soaked into the oil bath to start the hydrolysis reaction at 65 °C. At this step, an opaque-color solution was observed, suggested that the hydrolysis occurred. After 24-h aging, the reaction was forced to stop by quenching the flask with cold-water. The slurry was filtered and washed with deionized water, dried at 80 °C overnight and calcined at 550 °C for 5 h. The obtained catalyst was denoted as NMA-UH.

All catalysts were characterized by several techniques, including SEM-EDX, BET, XRD, H_2-TPR, and CO_2-TPD. More details about the characterization methods can be found in Supplementary Material, Section 2 (SM.S2).

Catalytic evaluation system

CO_2 methanation tests were carried out in a U-shape quartz reactor (i.d. 10 mm) placed in a furnace that allowed the temperature reaches 900 °C. The temperature was governed by a thermocouple K-type. Catalysts were packed between 2 layers of quartz wool, with the desired mass of each catalyst calculated based on its own density to achieve GHSV = 12,000 h^{-1}. Prior to methanation tests, catalysts were reduced *in-situ* at 900 °C in the 100 ml-H_2/Ar flow (5% vol/vol) for 1h, ramp 10 °C/min. Afterward, methanation flow consisting of H_2/CO_2/Ar (12/3/5) was fed into the reactor at a total flow rate of 100 cc/min. The reaction was performed in the range of 250–450 °C, 50 °C/step, and held at a steady condition for 30 min for each step. The outlet was analyzed using a gas chromatograph (490Varian Micro-GC) with a thermal conductivity detector (TCD).

The catalytic performance was evaluated via CO_2 conversion, CH_4 selectivity and Carbon balance (C_b). TOF values were reported (TOF expresses the number of converted CO_2 molecules (N_{CO_2}) per exposed Ni atoms (N_{Ni}) per unit time (s) [39]) for all catalysts.

The setup and all detailed calculations can be found in SM.S1 (Fig. 1, Eqs. 1-5). The catalyst stability was examined on the best catalyst by time-on-stream run for 27.5 h at 300 °C.

Results and discussion

Catalyst characterizations

Scanning electron microscopy (SEM)

Visually, all 3 mixed-oxides catalysts owned identical morphology; in specific, a solid form after thermal treatment at 550 °C could be seen. This is in agreement with previous observations [40].

Regarding EDS results (SM.S2, Table 1), the content of Ni on NMA-IMP was lower than that of both NMA-CP and NMA-UH. This loss was counted from the solution evaporation during the impregnation process. It is worth noticing that EDS mapping presents a small region of catalyst surface, and the fact that Ni-species are easily aggregated to form cluster/bulk through impregnating step (by the uneven distribution of Ni-species onto MgAl-HT surface); consequently, at some points, the Ni content detected by EDS is lower, but in another region, it could be much higher. In the cases of NMA-CP and NMA-UH, Ni was easily incorporated into HT-framework, resulting in more homogeneous inter-dispersion. It will be proved in H_2-TPR results later, in which the broader peak with higher intensity of Ni–O–Al (around 800 °C) was observed in the reduction profiles of NMA-CP and NMA-UH, while the lower intensity of the corresponding peak, alongside the appearance of more NiO-bulk species (broader band around 400–550 °C), could be seen on the TPR profile of NMA-IMP.

Low-temperature N_2 sorption

All isotherms of the calcined catalysts are of type IV according to IUPAC categorization [41]; surprisingly, different types of hysteresis loops were seen. NMA-CP presented H_3 type, typical of mesoporous materials, NMA-UH exhibited H_1 type with more layers in the catalyst structure. Furthermore, NMA-IMP seems to be different (SM.S2, Fig. 2). Thus, it is possible to state that the hydrolysis of urea in the presence of ionic metals generated catalysts with more layers in the structure compared to the traditional routes.

Please cite this article as: Nguyen-Quang M et al., On the influence of the preparation routes of NiMgAl-mixed oxides derived from hydrotalcite on their CO_2 methanation catalytic activities, International Journal of Hydrogen Energy, https://doi.org/10.1016/j.ijhydene.2022.08.278

Table 1 – Physicochemical and redox properties of the catalysts.

Catalysts		NMA-CP	NMA-UH	NMA-IMP
BET analysis				
BET surface area [m^2/g]		165	189	133
Pore volume V_p [cm^3/g_{cat}][a]		0.36	0.59	0.27
Mean pore diameter r_p [nm]		9.08	12.85	8.32
H_2-TPR analysis				
Total H_2 consumption [mmol/g_{cat}]		4.34	5.86	3.36
Peak consumption [mmol/g_{cat}]	399–424 °C	0.003	0.04	0.51
	700–722 °C	2.743	3.86	1.10
	790–808 °C	1.594	1.96	1.75
Distribution (%)	399–424 °C	0.1	0.64	15.1
	700–722 °C	63.2	65.8	32.8
	790–808 °C	36.7	33.5	52.1
CO_2-TPD analysis				
Total Basicity [μmol/g_{cat}]		56.8	277.9	162.0
Distribution (%)	Weak	22.5	48.9	8.7
	Medium	60.0	29.5	52.2
	Strong	17.5	21.6	39.1
XRD analysis				
NiO particle size [nm] Calcined catalysts		2.8	2.9	4.5
SEM analysis				
Ni^0 particle size [nm] Reduced catalysts		17.5	12.2	22.5
Ni^0 particle size [nm] Spent catalysts		32	31	38
Dispersion (%)		5.8	7.9	4.5
Carbon Balance ($C_{b,}$ %)$^{300°C}$		94.8	92.4	93.9

[a] Pore volume determined from the adsorption isotherms by BJH method.

The N_2 adsorption-desorption data of the calcined catalysts are presented in Table 1. According to the BET analysis, the specific surface area (SSA) of the prepared catalysts is considerably influenced by the preparation method. The SSA of NMA prepared by impregnating was the lowest (133 m^2/g), while the value of NMA-UH was higher (189 m^2/g). The partial blocking of pores by the growth of particle size caused during the impregnation step could be the reason for NMA-IMP owning the lowest SSA. The measured SSA, in this case, was supposed to be dominantly contributed by the smaller pores - further discussion in section *3.1.3. Powder X-ray diffraction (XRD)*. In comparison to NMA-CP and NMA-UH, where Ni-species were introduced into the framework more directly with uniform interdispersion, as the corollary, the pores are more open. This is evidenced by the larger mean-pore-diameter (r_p) and pore volume (V_p) of NMA-CP and NMA-UH (see Table 1). It should be noted that NMA-UH possesses the biggest (r_p) and (V_p) in the three-catalyst series, at 12.85 nm and 0.59 cm^3/g_{cat}, respectively.

Powder X-ray diffraction (XRD)

Catalyst diffractograms reveal several prominent reflections at $2\theta = 37.5°$, 43.3°, 63.2°, 75.3°, and 79.5°. These peaks correspond to the diffraction of NiO-lattice planes (111), (200), (220), (311), and (222), which are consistent with the prior study [42]. According to Debek et al. [43], the occurrence of three reflections at $2\theta \approx 36°$, 43.5°, and 63.2° is similarly associated with the periclase-like structure of Ni–Mg–Al mixed oxides (ICOD 00-045-0946). Furthermore, some authors [44–46] stated that $NiMgO_2$ could also show the characteristic diffraction peaks at $2\theta = 37°$, 43.3° and 63°, in which the main reflection was localized in the range of $2\theta \approx 42.2°$ to 43.6°. The reflections of MgO [45] were recorded at the same position; as a result, it is logical to assume that a $MgNiO_2$ solid solution coexists with the MgO crystal phase in our catalyst. The reflections of $NiAl_2O_4$ phases, on the other hand, can position at $2\theta = 37°$, 43°, 63.5°, according to Ref. [45] (see SM.S2, Fig. 3). The absence of segregated phases (NiO, MgO, Al_2O_3) in all catalysts suggested that the mixed oxides were solid solutions containing transition metal cations.

In terms of peak shape and intensity, the NMA-IMP diffractogram showed sharper peaks with higher intensity than NMA-CP and NMA-UH, implying that the NMA-IMP has a larger NiO particle size. This was validated by determining NiO particle size (L) using the using Scherrer equation (SM.S2, Eq. 6); the results are shown in Table 1, with the particle size classified as NMA-CP (2.8 nm), NMA-UH (2.9 nm), and NMA-IMP (4.5 nm); this confirmed the bigger particle sizes were presented in NMA-IMP catalysts.

In correlation to BET surface area results, where NMA-IMP showed the lowest value at 133 m^2/g, in fact, it is commonly acknowledged that increasing crystalline size reduces the surface area [47–50]. Nitrogen molecules are unable to access the pores due to the confinement and coverage of pores by bigger Ni-particles on the surface. The results were proven by a diffractogram of NMA-IMP (SM.S2, Fig. 3-blue line), which revealed that it had the highest crystallinity among the others (see Fig. 1).

Study of the reducibility of catalysts (H_2-TPR)

Fig. 2 shows the H_2-TPR profiles of all catalysts. The synthesis of HT via different methods resulted in the formation of different Ni-species, which is indicated by diverse reduction peaks.

The effects of the applied preparation methods are first particularly evident below 550 °C. For these catalysts, four reduction peaks were observed: ca. 207 °C (I), around 289 °C (II), about 397 °C (III), and the last one at 506 °C (IV). They are attributed to the isolated NiO and NiO un-uniformly scattered on the support surface - (I) and (II) [51], and the reduction in free-bulk NiO/well-dispersed NiO and bulk NiO weakly interacting with the Mg(Al)O phase - (III) and (IV) [52], respectively.

The shifts of peaks could be observed for the NMA-UH compared to NMA-UH. In detail, the reduction peak (I) of NMA-UH was relocated 20 °C lower to ca.190 °C, peak (II) was positioned at 282 °C (shifted by 7 °C to the left), peak (III) was situated at 395 °C, and (IV) was shifted to 470 °C (36 °C shift). Together with the increased intensities of these reduction peaks, this suggested that the hydrolysis process during preparation weakened Ni-bonds while generating weaker NiO species on the surface.

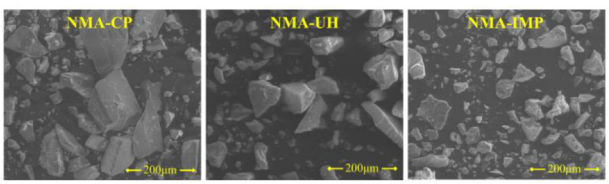

Fig. 1 – SEM images of calcined catalysts.

Please cite this article as: Nguyen-Quang M et al., On the influence of the preparation routes of NiMgAl-mixed oxides derived from hydrotalcite on their CO_2 methanation catalytic activities, International Journal of Hydrogen Energy, https://doi.org/10.1016/j.ijhydene.2022.08.278

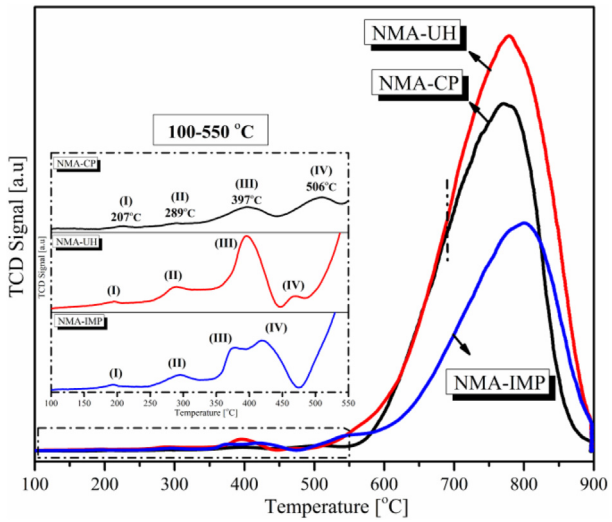

Fig. 2 – H_2-TPR profiles of NMA with different preparation methods.

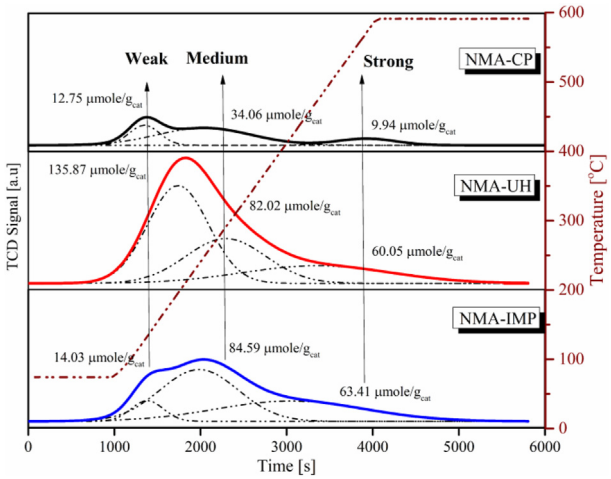

Fig. 3 – CO_2-TPD profiles of NMA with different preparation methods.

The same observation could be made on NMA-IMP, as all reduction peaks in this temperature range migrated to lower positions; however, peak profiles for (III) and (IV) - blue line, were distinctive. These peaks belong to the reduction of NiO-species in the form of bulk/cluster and/or sintering, with broader bands and higher H_2-consumption (ca.15% distribution corresponding to 0.51 mmol/g_{cat}) compared to NMA-CP and NMA-UH at 0.1–0.6%, respectively, it revealed the presence of more NiO species on the NMA-IMP surface. The result was consistent with the BET and XRD observations.

The reduction of stoichiometric $NiAl_2O_4$ species [53] leads to prominent reduction peaks at high temperatures (about 800 °C and shoulder peaks at 720 °C) for all three catalysts. The intensity of this peak was seen highest for NMA-UH, demonstrating the homogenous inter-dispersion of cations in the brucite layers of hydrotalcite, which give rise to the number of strong interactions of the active metal with hydrotalcite-derived material (Ni–O–Al). The peak positions for NMA-CP and NMA-UH are identical, but in the case of NMA-IMP, there is a slight shift towards higher temperatures, and at the same time, the area of the TCD profile is smaller. This suggests that impregnating Ni onto MgAl-HT resulted in a lower number of strong Ni-HT framework interactions, but the interactions are more robust; Ni-species present on this catalyst are in more difficult-to-reduce states. Table 1 reports the data regarding H_2 consumption for all catalysts.

The basicity of catalysts (CO_2-TPD)

CO_2-TPD profiles of hydrotalcite-derived materials are shown in Fig. 3, in which three CO_2 desorption peaks corresponding to weak, medium-strength and strong basic sites can be seen in agreement with the literature [54–56].

CO_2 desorption from the surface basic OH-group (hydrogen carbonate species) was allocated to the earliest desorption peak (at 130–195 °C), whereas CO_2 desorption from metal-oxygen pairs (M^{n+} - O^{2-} pairs) assigned to the medium-strength basic sites was centered around 270–340 °C. Finally, as found for hydrotalcite-derived catalysts via the CO_2-bond on the low oxygen coordination [57], CO_2 desorbed from strong-basic sites at higher temperatures (470–550 °C). The same observations have been reported in the literature, with hydrotalcite-derived materials showing three desorption peaks in the temperature range of 100–600 °C (Fig. 3).

Total basicity was computed using Gaussian fitting to integrate the desorption profile, which was deconvoluted from three basic site contributions (weak, medium, and strong). Catalysts presented a diverse distribution of weak, medium, and strong basic sites, where the strong basic sites contributed more on NMA-IMP (approximately 39%) and roughly the same for both NMA-UH and NMA-UH (varying from 17 to 21%). On NMA-UH, there was a clear difference in the generation of weak sites, with 48% of distribution, whereas it was approximately 8% on NMA-IMP catalyst. One can note that the calculated total basicity increases from 56.8 μmol/g_{cat}, 162 μmol/g_{cat} to 277 μmol/g_{cat} for NMA-CP, IMP to UH accordingly (Table 1). Also, the total basicity of NMA-UH is 5-time higher than NMA-CP. It was widely accepted that there is a linear correlation between weak, medium site distribution and CO_2 conversion [55]; therefore, NMA-UH is expected to deliver a high activity in our study.

It is known that urea is a weak Brønsted base with a pK_b of 13.8, it has strong solubility, and urea hydrolysis occurs slowly, resulting in low supersaturation during precipitation. Ammonium carbonate is formed when it decays (Eq. (3)):

$$H_2N\text{-}(C{=}O){-}NH_2 + 2H_2O \rightarrow 2NH_4^+ + CO_3^{2-} \quad \text{(Eq. 3)}$$

In fact, according to the literature [58], the hydrolysis of urea proceeds in two steps, the formation of ammonium cyanate (NH_4CNO) (Eq. (4)) as the rate-determining step:

$$H_2N\text{-}(C{=}O){-}NH_2 \rightarrow NH_4^+ + NCO^- \quad \text{(Eq. 4)}$$

And the fast hydrolysis of the cyanate to ammonium carbonate (Eq. (5)) and/or possibly weak H_2CO_3 in basic medium (Eq. (6)), in which H_2CO_3 will be further segregated into $2H^+$ and CO_3^{2-} in such medium.

Please cite this article as: Nguyen-Quang M et al., On the influence of the preparation routes of NiMgAl-mixed oxides derived from hydrotalcite on their CO_2 methanation catalytic activities, International Journal of Hydrogen Energy, https://doi.org/10.1016/j.ijhydene.2022.08.278

$$NCO^- + 2H_2O \rightarrow NH_4^+ + CO_3^{2-} \quad \text{(Eq. 5)}$$

$$NCO^- + 2H^+ + 2H_2O \rightarrow NH_4^+ + H_2CO_3 \quad \text{(Eq. 6)}$$

This potentially indicated that NMA formed through the hydrolysis in basic medium will consequently generate more basicity and thus facilitate CO_2 activation, giving better catalytic activity.

Catalytic performance

The catalytic activity is reported in Fig. 4 for all catalysts as a function of temperature. The continuous lines show the registered CO_2 conversion, whereas the dashed lines represent CH_4 selectivity.

As it can be observed, catalytic activities toward CO_2 methanation were moderate at 250 °C, suggesting that the reaction was slowly initiated, as discussed before. Notwithstanding this, the effects of preparation procedures on CO_2 conversion and CH_4 selectivity can be realized. A conversion of 20% was found for the catalyst synthesized via urea hydrolysis, while for NMA-CP and NMA-IMP, it was much lower (around 6%). Regarding CH_4 selectivity, NMA-UH showed a good value (about 99%) at this temperature, but it is not the case for NMA-CP or NMA-IMP.

Up to 300 °C, all catalysts showed an improvement in the catalytic performance, with NMA-UH being the best as expected. According to obtained results, NMA-UH showed more than 60% gain in CO_2 conversion, from 20% to around 82%, while NMA-CP had a smaller rise to 46%, and for NMA-IMP, it was seen at 34% in CO_2 conversion. When temperatures were further increased to 350 °C, all conversions reached a higher value, with NMA-UH obtaining an 88.5%, followed by NMA-CP (83.1%) and NMA-IMP (79.2%). This demonstrated that urea hydrolysis-derived catalysts could promote CO_2 methanation at lower temperatures.

Summary data from Table 1 and Fig. 5 show that NMA-UH presents the highest surface area (189 m^2/g) and the biggest mean pore diameter of 12.85 nm, as well as the highest total

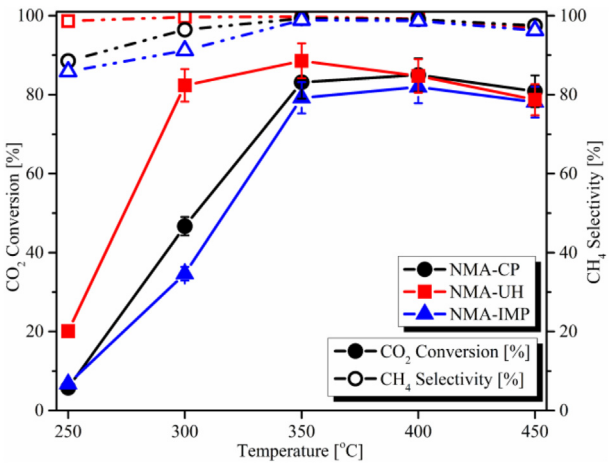

Fig. 4 – CO_2 Conversion and CH_4 selectivity of catalysts versus temperatures.

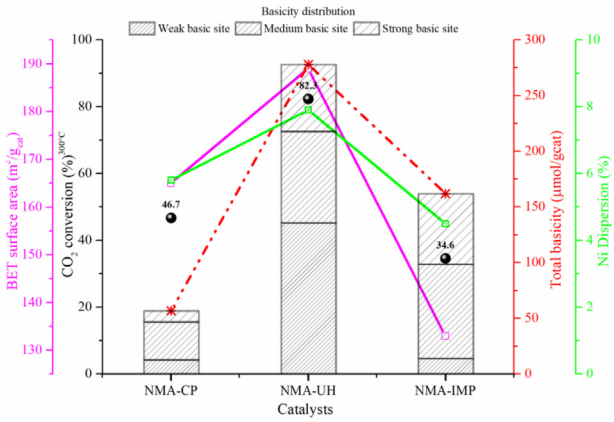

Fig. 5 – Correlation between the CO_2 conversion and catalyst aspects.

basicity (278μmol/g_{cat}) with 218μmol/g_{cat} contribution from weak and medium sites. It is worth mentioning that this contribution of weak and medium strength sites approximately equals to the total basicity of NMA-CP and NMA-IMP put together. As widely reported by Refs. [55,59–61], the combinatorial effect of Ni and basic sites can strongly promote catalytic activity. These are crucial factors for achieving a high level of catalytic activity. Furthermore, SEM mapping on reduced catalysts revealed the smallest Ni^0 particle of 12.2 nm, which correlate with the highest Ni-dispersion (%). The best behavior of NMA-UH, therefore, was pointed out by all of the aforesaid features. On the contrary, with the lowest surface area, the minor proportion of weak-and-medium basic sites, the most Ni species difficult to reduce, with the largest Ni^0 particle size (22 nm) (cp. Table 1), it is no surprise that NMA-IMP performed the worst among the three studied catalysts. The CH_4 selectivity at 300°C–350 °C witnessed superior 99–99.8% of values.

To compare with the literature, the catalytic activity of NMA-UH at 300 °C, Table 2 is presented.

Because of thermodynamic limitation (see SM.S2, Fig. 4), the catalytic activities decreased upwards of 400 and 450 °C; i.e., NMA-CP, NMA-UH, and NMA-IMP showed lower CO_2 conversion at ca. 80.8%, 78.7%, and 78.1% with 97.5%, 96.9% and 96.2% of CH_4 selectivity at 450 °C, respectively. As the temperature increases above 400°C–450 °C, the RWGS reaction ($CO_2 + H_2O \rightarrow CO + H_2$, $\Delta H^0_{298K} = 41kJ/mol$, (Eq. 7)) becomes more favorable; therefore, a small amount of carbon monoxide is generated as a byproduct. This is one of the reasons the reaction was not examined at temperatures higher than 450 °C.

Moreover, a time-on-stream (TOS) run for NMA-UH at 300 °C for 27.5 h was performed to assess the catalyst's stability. Fig. 6 depicts the results.

The TOS run showed a good agreement with catalytic performance results with ca. 81% CO_2 conversion and 99.5% selectivity recorded. After a 27.5-h test, both CO_2 conversion and selectivity remained stable, with no significant changes suggesting that the NMA-UH catalyst has remarkable stability. TOF calculation suggested that NMA-UH is the one that allows CO_2 molecules to be converted more on one Ni-site. The TOF values for all catalysts are listed 0.25 (s^{-1}) < 0.29 (s^{-1}) < 0.82 (s^{-1}), corresponding to NMA-IMP < NMA-CP < NMA-UH.

Please cite this article as: Nguyen-Quang M et al., On the influence of the preparation routes of NiMgAl-mixed oxides derived from hydrotalcite on their CO_2 methanation catalytic activities, International Journal of Hydrogen Energy, https://doi.org/10.1016/j.ijhydene.2022.08.278

Table 2 – Comparison of catalytic activity with some available data.

Catalysts[a]	Preparation method	Feed H_2/CO_2	GHSV (h^{-1})	CO_2 Conv. (%)	CH_4 Sel. (%)	Ref.
Ni15/Cu1	CP	4	12,000	62	99	[62]
Ni15/V2	CP	4	12,000	75	99	[63]
Ni15	CP	4	12,000	63	99	[64]
Ni15/La2	CP	4	12,000	75	98	
Ni15	UH	4	12,000	82	99	This work

[a] Hydrotalcite type, Ni/promoter (wt.%/wt.%).

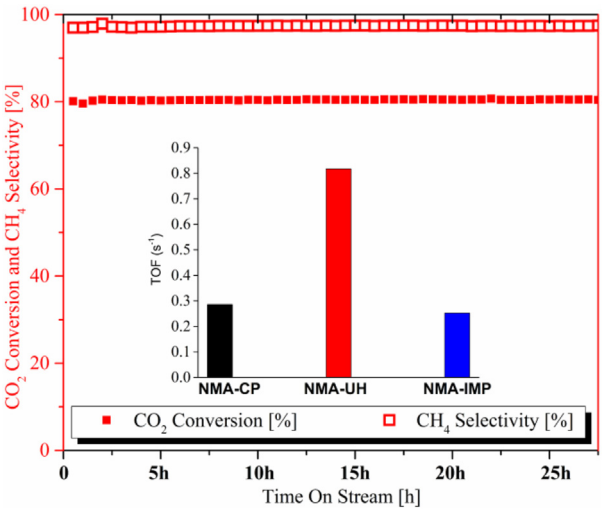

Fig. 6 – TOS run of NMA-UH at 300 °C and TOF calculation for all catalysts.

Spent catalyst evaluation

Used catalysts were characterized further using XRD and SEM analysis. XRD diffractograms and SEM images are given in SM.S3, Figs. 6 and 8.

XRD revealed no C-deposition peak at about $2\theta = 20°$, indicating no C-deposition form existed on the catalyst surface. SEM analysis revealed the increased particle size compared to the reduced catalysts suggesting the active site suffered aggregation following the reaction. Carbon balance (C_b) was also calculated (SM.S2, Fig. 5). Data at 300 °C (Table 1) showed the unclosed C_b. The fact that XRD identified no C-deposition but the C_b are unclosed suggests that some types of C species may exist as byproducts or intermediates. Carbon could be present in the form of carbonate, hydrogen carbonate, or carbonyl; however, it could not be further transformed during the reaction, therefore remaining on the catalyst surface and, as a result, C_b was opened.

Conclusions

In this study, NiMgAl-Hydrotalicte was synthesized, evaluated under CO_2 methanation, and compared to the catalysts prepared by co-precipitation and impregnation. The results reveal that the preparation process has a significant impact on both physicochemical and redox parameters, as well as catalytic performance. The catalyst synthesized via urea hydrolysis showed the best activity, with an average conversion rate of 82.3% and a selectivity of 99.8% for CH_4 at 300 °C. There is a possibility of tuning synthesis parameters such as temperature and aging time to improve the catalytic performance further.

Declaration of competing interest

The authors declare that they have no known competing financial interests or personal relationships that could have appeared to influence the work reported in this paper.

Acknowledgments

This work has been received support from the European Research Framework Program: H2020 | Marie Skłodowska-Curie Action (MSCA), PIONEER project: plasma catalysis for CO_2 recycling (Grant no. 813393).

Appendix A. Supplementary data

Supplementary data to this article can be found online at https://doi.org/10.1016/j.ijhydene.2022.08.278.

REFERENCES

[1] Conti J, Holtberg P, Diefenderfer J, LaRose A, Turnure JT, Westfall L. International energy Outlook 2016 with projections to 2040. https://doi.org/10.2172/1296780; 2016.
[2] Rönsch S, Schneider J, Matthischke S, Schlüter M, Götz M, Lefebvre J, et al. Review on methanation – from fundamentals to current projects. Fuel 2016;166:276–96. https://doi.org/10.1016/j.fuel.2015.10.111.
[3] Sabatier P, Senderens JB. Direct hydrogenation of oxides of carbon in presence of various finely divided metals. C R Acad Sci 1902;134:689–91.
[4] Vogt C, Monai M, Kramer GJ, Weckhuysen BM. The renaissance of the Sabatier reaction and its applications on Earth and in space. Nature Catalysis 2019;2:188–97. https://doi.org/10.1038/s41929-019-0244-4.
[5] Mohd Ridzuan ND, Shaharun MS, Anawar MA, Ud-Din I. Ni-based catalyst for carbon dioxide methanation: a review on performance and progress. Catalysts 2022;12. https://doi.org/10.3390/catal12050469.
[6] Guo X, Traitangwong A, Hu M, Zuo C, Meeyoo V, Peng Z, et al. Carbon dioxide methanation over nickel-based catalysts supported on various mesoporous. Material. Energy & Fuels 2018;32:3681–9. https://doi.org/10.1021/acs.energyfuels.7b03826.
[7] Lv C, Xu L, Chen M, Cui Y, Wen X, Li Y, et al. Recent progresses in constructing the highly efficient Ni based catalysts with advanced low-temperature activity toward CO2 methanation. https://doi.org/10.3389/fchem.2020.00269; 2020.
[8] Ren J, Mebrahtu C, Palkovits R. Ni-based catalysts supported on Mg–Al hydrotalcites with different morphologies for CO2 methanation: exploring the effect of metal–support

interaction. Catal Sci Technol 2020;10:1902–13. https://doi.org/10.1039/C9CY02523E.

[9] Huynh HL, Yu Z. CO2 methanation on hydrotalcite-derived catalysts and structured reactors: a review. Energy Technol 2020;8:1901475. https://doi.org/10.1002/ente.201901475.

[10] McKenzie AL, Fishel CT, Davis RJJJoC. Investigation of the surface structure and basic properties of calcined hydrotalcites. 1992. p. 547–61. https://doi.org/10.1016/0021-9517(92)90306-3. 138.

[11] Tichit D, Lhouty MH, Guida A, Chiche BH, Figueras F, Auroux A, et al. Textural properties and catalytic activity of hydrotalcites. J Catal 1995;151:50–9. https://doi.org/10.1006/jcat.1995.1007.

[12] Corma A, Fornes V, Rey F. Hydrotalcites as base catalysts: influence of the chemical composition and synthesis conditions on the dehydrogenation of isopropanol. J Catal 1994;148:205–12. https://doi.org/10.1006/jcat.1994.1202.

[13] Di Cosimo JI, Díez VK, Xu M, Iglesia E, Apesteguía CR. Structure and surface and catalytic properties of Mg-Al basic oxides. J Catal 1998;178:499–510. https://doi.org/10.1006/jcat.1998.2161.

[14] Schaper H, Berg-Slot JJ, Stork WHJ. Stabilized magnesia: a novel catalyst (support) material. Appl Catal 1989;54:79–90. https://doi.org/10.1016/S0166-9834(00)82356-8.

[15] Cavani F, Trifirò F, Vaccari A. Hydrotalcite-type anionic clays: preparation, properties and applications. Catal Today 1991;11:173–301. https://doi.org/10.1016/0920-5861(91)80068-K.

[16] Tan P, Gao Z, Shen C, Du Y, Li X, Huang W. Ni-Mg-Al solid basic layered double oxide catalysts prepared using surfactant-assisted coprecipitation method for CO2 reforming of CH4. Chin J Catal 2014;35:1955–71. https://doi.org/10.1016/S1872-2067(14)60171-6.

[17] Martínez-Lozano G, Kryshtab T, Hesiquio Garduño M, Kryvko A. Synthesis and characterization of Ni/Mg/Al mixed oxides obtained by Co-precipitation. MRS Online Proc Libr 2011;1372:13–20. http://10.1557/opl.2012.126.

[18] Prince J, Montoya A, Ferrat G, Valente JS. Proposed general Sol–Gel method to prepare Multimetallic layered double hydroxides: synthesis, characterization, and Envisaged application. Chem Mater 2009;21:5826–35. https://doi.org/10.1021/cm902741c.

[19] Valente J, Sánchez-Cantú M, Cortez J, Montiel R, Bokhimi X, López-Salinas E. Preparation and characterization of Sol–Gel MgAl hydrotalcites with Nanocapsular morphology. J Phys Chem C - J PHYS CHEM C 2006;111. http://10.1021/jp065283h.

[20] Lopez T, Bosch P, Ramos E, Gomez R, Novaro O, Acosta D, et al. Synthesis and characterization of Sol–Gel hydrotalcites. Structure and Texture. Langmuir 1996;12:189–92. http://10.1021/la940703s.

[21] Gardner E, Huntoon K, Pinnavaia T. Direct synthesis of Alkoxide-intercalated derivatives of Hydrocalcite-like layered double hydroxides: precursors for the formation of colloidal layered double Hydroxide Suspensions and transparent Thin Films. Advanced Materials - ADVAN MATER 2001;13. https://doi.org/10.1002/1521-4095(200108)13:163.0.CO;2-R.

[22] Rao MM, Reddy BR, Jayalakshmi M, Jaya VS, Sridhar B. Hydrothermal synthesis of Mg–Al hydrotalcites by urea hydrolysis. Mater Res Bull 2005;40:347–59. https://doi.org/10.1016/j.materresbull.2004.10.007.

[23] Bankauskaite A, Baltakys K. The hydrothermal synthesis of hydrotalcite by using different partially Soluble and insoluble in water Mangesium and Aluminium components. Sci Sinter 2011;43. http://10.2298/SOS1103261B.

[24] Xu ZP, Lu GQ. Hydrothermal synthesis of layered double hydroxides (LDHs) from mixed MgO and Al2O3: LDH formation Mechanism. Chem Mater 2005;17:1055–62. https://doi.org/10.1021/cm048085g.

[25] Mészáros S, Halász J, Kónya Z, Sipos P, Pálinkó I. Reconstruction of calcined MgAl- and NiMgAl-layered double hydroxides during glycerol dehydration and their recycling characteristics. Appl Clay Sci 2013;80–81:245–8. https://doi.org/10.1016/j.clay.2013.04.010.

[26] Fetter G, Hernández F, Maubert AM, Lara VH, Bosch P. Microwave irradiation effect on hydrotalcite synthesis. J Porous Mater 1997;4:27–30. https://doi.org/10.1023/A:1009619005529.

[27] Benito P, Guinea I, Labajos F, Rives V. Microwave-assisted reconstruction of Ni,Al hydrotalcite-like compounds. J Solid State Chem 2008;181:987–96. http://10.1016/j.jssc.2008.02.003.

[28] Rivera JA, Fetter G, Bosch P. Microwave power effect on hydrotalcite synthesis. Microporous Mesoporous Mater 2006;89:306–14. https://doi.org/10.1016/j.micromeso.2005.10.041.

[29] Fetter G, Bosch P, Hernandez FA. Synthesis of hydrotalcites using microwave irradiation. MRS Online Proc Libr 1996;454:235–9. https://doi.org/10.1557/PROC-454-235.

[30] Vial S, Ghanbaja J, Forano C. Precipitation of Zn2Al LDH by urease enzyme. Chem Commun 2006:290–2. https://doi.org/10.1039/B510470J.

[31] Naseem S, Gevers B, Boldt R, Labuschagné FJWJ, Leuteritz A. Comparison of transition metal (Fe, Co, Ni, Cu, and Zn) containing tri-metal layered double hydroxides (LDHs) prepared by urea hydrolysis. RSC Adv 2019;9:3030–40. https://doi.org/10.1039/C8RA10165E.

[32] Liu Z, Ma R, Ebina Y, Iyi N, Takada K, Sasaki T. General synthesis and delamination of highly crystalline transition-metal-Bearing layered double hydroxides. Langmuir 2007;23:861–7. https://doi.org/10.1021/la062345m.

[33] Sreenavya A, Ganesh V, Venkatesha NJ, Sakthivel A. Hydrogenation of biomass derived furfural using Ru-Ni-Mg–Al-hydrotalcite material. Biomass Conversion and Biorefinery; 2022. https://doi.org/10.1007/s13399-022-02641-8.

[34] Adachi-Pagano M, Forano C, Besse J-P. Synthesis of Al-rich hydrotalcite-like compounds by using the urea hydrolysis reaction—control of size and morphology. J Mater Chem 2003;13:1988–93. https://doi.org/10.1039/B302747N.

[35] Zeng H-Y, Deng X, Wang YJ, Liao KB. Preparation of Mg-Al hydrotalcite by urea method and its catalytic activity for Transesterification. AIChE J 2009;55:1229–35. https://doi.org/10.1002/aic.11722.

[36] Bian L, Wang W, Xia R, Li Z. Ni-based catalyst derived from Ni/Al hydrotalcite-like compounds by the urea hydrolysis method for CO methanation. RSC Adv 2016;6:677–86. https://doi.org/10.1039/C5RA19748A.

[37] Kloprogge JT, Hickey L, Trujillano R, Holgado MJ, San Román MS, Rives V, et al. Characterization of intercalated Ni/Al hydrotalcites prepared by the partial decomposition of urea. Cryst Growth Des 2006;6:1533–6. https://doi.org/10.1021/cg0504612.

[38] He L, Lin Q, Liu Y, Huang Y. Unique catalysis of Ni-Al hydrotalcite derived catalyst in CO2 methanation: cooperative effect between Ni nanoparticles and a basic support. J Energy Chem 2014;23:587–92. https://doi.org/10.1016/S2095-4956(14)60144-3.

[39] Boudart M. Turnover rates in Heterogeneous catalysis. Chem Rev 1995;95:661–6. https://doi.org/10.1021/cr00035a009.

[40] Wang Q, Tay HH, Guo Z, Chen L, Liu Y, Chang J, et al. Morphology and composition controllable synthesis of Mg–Al–CO3 hydrotalcites by tuning the synthesis pH and the CO2 capture capacity. Appl Clay Sci 2012;55:18–26. https://doi.org/10.1016/j.clay.2011.07.024.

[41] Eddaoudi M. Characterization of Porous Solids and Powders: surface Area, Pore Size and Density By S. Lowell (Quantachrome Instruments, Boynton Beach), J. E. Shields

Please cite this article as: Nguyen-Quang M et al., On the influence of the preparation routes of NiMgAl-mixed oxides derived from hydrotalcite on their CO_2 methanation catalytic activities, International Journal of Hydrogen Energy, https://doi.org/10.1016/j.ijhydene.2022.08.278

(C. W. Post Campus of Long Island University), M. A. Thomas, and M. Thommes (Quantachrome In-struments). Kluwer Academic Publishers: dordrecht, The Netherlands. 2004. xiv + 348 pp. $159.00. ISBN 1-4020-2302-2. J Am Chem Soc 2005;127:14117. https://doi.org/10.1021/ja041016i.
[42] Rives V. Characterisation of layered double hydroxides and their decomposition products. Mater Chem Phys 2002;75:19–25. http://10.1016/S0254-0584(02)00024-X.
[43] Dębek R, Motak M, Duraczyska D, Launay F, Galvez ME, Grzybek T, et al. Methane dry reforming over hydrotalcite-derived Ni–Mg–Al mixed oxides: the influence of Ni content on catalytic activity, selectivity and stability. Catal Sci Technol 2016;6:6705–15. http://10.1039/C6CY00906A.
[44] Broda M, Kierzkowska AM, Baudouin D, Imtiaz Q, Copéret C, Müller CR. Sorbent-Enhanced Methane Reforming over a Ni–Ca-Based, Bifunctional Catalyst Sorbent. ACS Catal 2012;2:1635–46. http://10.1021/cs300247g.
[45] Zhan Y, Han J, Bao Z, Cao B, Li Y, Street J, et al. Biogas reforming of carbon dioxide to syngas production over Ni-Mg-Al catalysts. Mol Catal 2017;436:248–58. https://doi.org/10.1016/j.mcat.2017.04.032.
[46] Zhu Y, Zhang S, Chen B, Zhang Z, Shi C. Effect of Mg/Al ratio of NiMgAl mixed oxide catalyst derived from hydrotalcite for carbon dioxide reforming of methane. Catal Today 2016;264:163–70. https://doi.org/10.1016/j.cattod.2015.07.037.
[47] Kovanda F, Koloušek D, Zlámalová Cílová Z, Hulínský V. Crystallization of synthetic hydrotalcite under hydrothermal conditions. Appl Clay Sci 2005;28:101–9. https://doi.org/10.1016/j.clay.2004.01.009.
[48] Chaillot D, Bennici S, Brendlé J. Layered double hydroxides and LDH-derived materials in chosen environmental applications: a review. Environ Sci Pollut Control Ser 2021;28:24375–405. https://doi.org/10.1007/s11356-020-08498-6.
[49] Kołbuk D, Ciechomska M, Jeznach O, Sajkiewicz P. Effect of crystallinity and related surface properties on gene expression of primary fibroblasts. RSC Adv 2022;12:4016–28. https://doi.org/10.1039/D1RA07237D.
[50] Raj KJS. Viswanathan BJIjocSAI, physical, theoretical, analytical. Effect of surface area, pore volume and particle size of P25 titania on the phase transformation of anatase to rutile 2009;48:1378–82.
[51] Perez-Lopez OW, Senger A, Marcilio NR, Lansarin MA. Effect of composition and thermal pretreatment on properties of Ni–Mg–Al catalysts for CO2 reforming of methane. Appl Catal, A 2006;303:234–44. https://doi.org/10.1016/j.apcata.2006.02.024.
[52] Tichit D, Medina F, Coq B, Dutartre R. Activation under oxidizing and reducing atmospheres of Ni-containing layered double hydroxides. Appl Catal Gen 1997;159:241–58. https://doi.org/10.1016/S0926-860X(97)00085-9.
[53] Ichikuni N, Murata D, Shimazu S, Uematsu T. Promoting effect of NiAl2O4 for supported Ni particles on sprayed Ni/Al2O3 catalysts. Catal Lett 2000;69:33–6. https://doi.org/10.1023/A:1019009620601.
[54] Świrk K, Galvez M, Motak M, Grzybek T, Rønning M, Da Costa P. Yttrium promoted Ni-based double-layered hydroxides for dry methane reforming. J CO2 Util 2018;27:247–58. https://doi.org/10.1016/j.jcou.2018.08.004.
[55] Guo X, Gao D, He H, Traitangwong A, Gong M, Meeyoo V, et al. Promotion of CO2 methanation at low temperature over hydrotalcite-derived catalysts-effect of the tunable metal species and basicity. Int J Hydrogen Energy 2021;46:518–30. https://doi.org/10.1016/j.ijhydene.2020.09.193.
[56] Wierzbicki D, Baran R, Dębek R, Motak M, Grzybek T, Gálvez ME, et al. The influence of nickel content on the performance of hydrotalcite-derived catalysts in CO2 methanation reaction. Int J Hydrogen Energy 2017;42:23548–55. https://doi.org/10.1016/j.ijhydene.2017.02.148.
[57] Prinetto F, Ghiotti G, Graffin P, Tichit D. Synthesis and characterization of sol–gel Mg/Al and Ni/Al layered double hydroxides and comparison with co-precipitated samples. Microporous Mesoporous Mater 2000;39:229–47. https://doi.org/10.1016/S1387-1811(00)00197-9.
[58] Shaw WHR, Bordeaux JJ. The Decomposition of Urea in Aqueous Media. J Am Chem Soc 1955;77:4729–33. https://doi.org/10.1021/ja01623a011.
[59] Xiao X, Wang J, Li J, Dai H, Jing F, Liu Y, et al. Enhanced low-temperature catalytic performance in CO2 hydrogenation over Mn-promoted NiMgAl catalysts derived from quaternary hydrotalcite-like compounds. Int J Hydrogen Energy 2021;46:33107–19. https://doi.org/10.1016/j.ijhydene.2021.07.163.
[60] Yin L, Chen X, Sun M, Zhao B, Chen J, Zhang Q, et al. Insight into the role of Fe on catalytic performance over the hydrotalcite-derived Ni-based catalysts for CO2 methanation reaction. Int J Hydrogen Energy 2021;47(11):7139–49. https://doi.org/10.1016/j.ijhydene.2021.12.057.
[61] Sun C, Świrk K, Wierzbicki D, Motak M, Grzybek T, Da Costa P. On the effect of yttrium promotion on Ni-layered double hydroxides-derived catalysts for hydrogenation of CO2 to methane. Int J Hydrogen Energy 2021;46:12169–79. https://doi.org/10.1016/j.ijhydene.2020.03.202.
[62] Summa P, Samojeden B, Motak M, Wierzbicki D, Alxneit I, Świerczek K, et al. Investigation of Cu promotion effect on hydrotalcite-based nickel catalyst for CO2 methanation. Catal Today 2022;384–386:133–45. https://doi.org/10.1016/j.cattod.2021.05.004.
[63] Świrk K, Summa P, Wierzbicki D, Motak M, Da Costa P. Vanadium promoted Ni(Mg,Al)O hydrotalcite-derived catalysts for CO2 methanation. Int J Hydrogen Energy 2021;46(34):17776–83. https://doi.org/10.1016/j.ijhydene.2021.02.172.
[64] Wierzbicki D, Debek R, Motak M, Grzybek T, Gálvez ME, Da Costa P. Novel Ni-La-hydrotalcite derived catalysts for CO2 methanation. Catal Commun 2016;83:5–8. https://doi.org/10.1016/j.catcom.2016.04.021.

Please cite this article as: Nguyen-Quang M et al., On the influence of the preparation routes of NiMgAl-mixed oxides derived from hydrotalcite on their CO_2 methanation catalytic activities, International Journal of Hydrogen Energy, https://doi.org/10.1016/j.ijhydene.2022.08.278